

Sensitivity of future collider facilities to WIMP pair production via effective operators and light mediators

Ning Zhou,¹ David Berge,² LianTao Wang,³ Daniel Whiteson,¹ and Tim Tait¹

¹*Department of Physics and Astronomy, University of California, Irvine, CA 92697*

²*GRAPPA Institute, University of Amsterdam, Netherlands*

³*Department of Physics, University of Chicago, Chicago, IL*

We present extrapolations of the current mono-jet searches at the LHC to potential future hadron collider facilities: LHC14, as well as pp colliders with $\sqrt{s} = 33$ or 100 TeV. We consider both the effective operator approach as well as one example of a light mediating particle.

PACS numbers:

Though the presence of dark matter in the universe has been well-established, little is known of its particle nature or its non-gravitational interactions. A vibrant experimental program is searching for a weakly interacting massive particle (WIMP), denoted as χ , and interactions with standard model particles via some as-yet-unknown mediator.

One critical component of this program is the search for pair-production of WIMPs at particle colliders, specifically $pp \rightarrow \chi\bar{\chi}$ at the LHC via some unknown intermediate state. If the mediator is too heavy to be resolved, the interaction can be modeled as an effective field theory with a four-point interaction, otherwise an explicit model is needed for the heavy mediator. As the final state WIMPs are invisible to the detectors, the events can only be seen if there is associated initial-state radiation of a standard model particle [1–3], see Fig 1, recoiling against the dark matter pair.

The LHC collaborations have reported limits on the cross section of $pp \rightarrow \chi\bar{\chi} + X$ where X is a hadronic jet [4, 5], photon [6, 7], and other searches have been repurposed to study the cases where X is a W [8] or Z boson [9, 10]. In each case, limits are reported in terms of the mass scale M_* of the unknown interaction expressed in an effective field theory [1–3, 11–19], though the limits from the mono-jet mode are the most powerful [20].

In this paper, we study the sensitivity of possible future proton-proton colliders in various configurations (see Table I) to WIMP pair production using the mono-jet final state. We consider both effective operators and one example of a real, heavy Z' -boson mediator.

ANALYSIS TECHNIQUE

The analysis of jet+ \cancel{E}_T events uses a sample of events with one or two high p_T jets and large \cancel{E}_T , with angular cuts to suppress events with two back-to-back jets (multi-jet background). The dominant remaining background is $Z \rightarrow \nu\bar{\nu}$ in association with jets, which is indistinguishable from the signal process of $\chi\bar{\chi}$ +jets.

The estimation of the background at large \cancel{E}_T is problematic in simulated samples, due to the difficulties of accurately modeling the many sources of \cancel{E}_T . The experimental results, therefore, rely on data-driven background estimates, typically extrapolating the $Z \rightarrow \nu\bar{\nu}$ contribution from $Z \rightarrow \mu\mu$ events with large Z boson p_T .

In this study, we begin from experimentally reported values [4, 5] of the background estimates and signal efficiencies (at $\sqrt{s} = 7$ TeV, $\mathcal{L} = 5 \text{ fb}^{-1}$, $\cancel{E}_T > 350$ GeV), and use simulated samples to extrapolate to higher center-of-mass

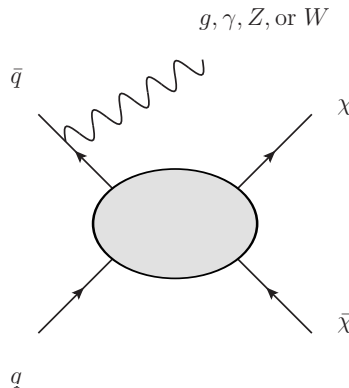


FIG. 1: Pair production of WIMPs ($\chi\bar{\chi}$) in proton-proton collisions at the LHC via an unknown intermediate state, with initial-state radiation of a standard model particle.

energies, where no data is currently available. At the higher collision energies and instantaneous luminosities of the proposed facilities, the rate of multi-jet production will also be higher, requiring higher \cancel{E}_T thresholds to cope with the background levels and the trigger rates.

Simulated Samples

We generate signal events as well as events for the dominant background $Z \rightarrow \nu\bar{\nu}$ +jets in MADGRAPH5 [26], with showering and hadronization by PYTHIA [27]. In each case, we generate events with zero or one hard additional colored parton and use the MLM scheme to match the matrix-element calculations of MADGRAPH5 to the parton shower evolution of PYTHIA.

Extrapolation

In the case of each potential facility, we must choose a \cancel{E}_T threshold for the analysis. For a given threshold at a specific facility, estimating the sensitivity of the jet+ \cancel{E}_T analysis requires

- the dark-matter signal efficiency
- an estimate of the $Z \rightarrow \nu\bar{\nu}$ +jets background
- the uncertainty of the $Z \rightarrow \nu\bar{\nu}$ +jets background.

For the signal efficiency, we modify the reported experimental efficiency at $\sqrt{s} = 7$ TeV [4, 5] to estimate the efficiency at a higher \cancel{E}_T cut. The estimated signal yield $N_{\text{sig}}(\sqrt{s}, \mathcal{L}, \cancel{E}_T > X)$ for a facility with center-of-mass energy \sqrt{s} and integrated luminosity \mathcal{L} is

$$N_{\text{sig}}(\sqrt{s}, \mathcal{L}, \cancel{E}_T > X) = \mathcal{L} \times \epsilon_0 \frac{\epsilon_{\cancel{E}_T > X}}{\epsilon_{\cancel{E}_T > 350}} \times \sigma(\sqrt{s})$$

where ϵ_0 is the published signal efficiency. In each case, the efficiency $\epsilon_{\cancel{E}_T > X}$ of a \cancel{E}_T threshold is measured at parton-level using the simulated samples, see Fig. 2, and the cross sections $\sigma(\sqrt{s})$ are leading order.

In the case of the background estimate, we extrapolate from the reported background estimate, denoted $N_{\text{bg}}^{\sqrt{s}=7, \mathcal{L}=5, \cancel{E}_T > 350}$, by scaling with an extrapolation factor E_b :

$$N_{\text{bg}}(\sqrt{s}, \mathcal{L}, \cancel{E}_T > X) = E_b \times N_{\text{bg}}^{\sqrt{s}=7, \mathcal{L}=5, \cancel{E}_T > 350}$$

where E_b is

$$E_b(\sqrt{s}, \mathcal{L}, \cancel{E}_T > X) = \frac{\mathcal{L}}{5 \text{ fb}^{-1}} \times \frac{\epsilon_{\cancel{E}_T > X}}{\epsilon_{\cancel{E}_T > 350}} \times \frac{\sigma(\sqrt{s})}{\sigma(\sqrt{s} = 7)}$$

accounting for the relative efficiency of a higher \cancel{E}_T cut and larger background cross sections at increased center-of-mass energies. The relative uncertainty on the background $N_{\text{bg}}^{\sqrt{s}=7, \mathcal{L}=5, \cancel{E}_T > 350}$ is scaled from the reported relative uncertainty, $(\frac{\Delta N_{\text{bg}}}{N_{\text{bg}}})^{\sqrt{s}=7, \mathcal{L}=5, \cancel{E}_T > 350}$, using the extrapolation factor E_b as given above:

$$\frac{\Delta N_{\text{bg}}}{N_{\text{bg}}}(\sqrt{s}, \mathcal{L}, \cancel{E}_T > X) = \frac{1}{\sqrt{E_b}} \left(\frac{\Delta N_{\text{bg}}}{N_{\text{bg}}} \right)^{\sqrt{s}=7, \mathcal{L}=5, \cancel{E}_T > 350}$$

Together, the background estimate with uncertainties and the dark-matter signal efficiencies allow us to calculate the power of the jet+ \cancel{E}_T analysis.

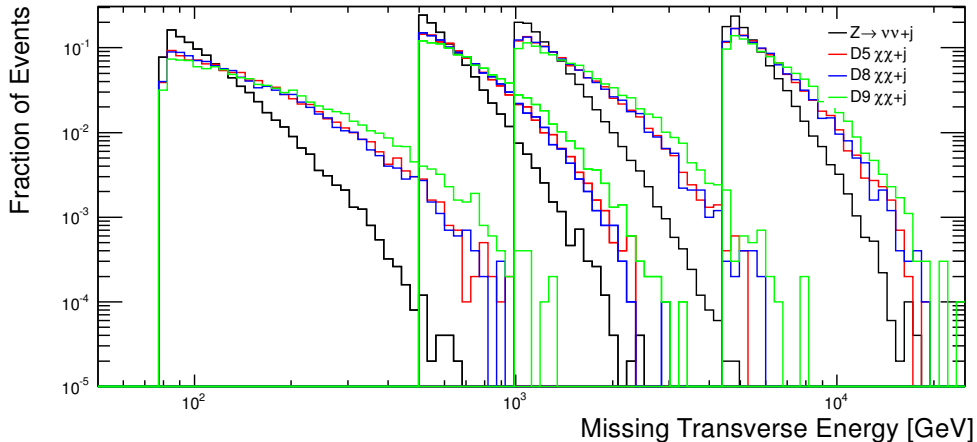


FIG. 2: Missing transverse energy for signal ($\chi\bar{\chi}$ +jets) and background ($Z \rightarrow \nu\bar{\nu}$ +jets) samples generated at $\sqrt{s}=7, 14, 33$ and 100 TeV with thresholds of 80, 500, 1000 and 4500 GeV, with $m_\chi = 10$ GeV.

TABLE I: Details of current and potential future pp colliders, including center-of-mass energy (\sqrt{s}), total integrated luminosity (\mathcal{L}), the threshold in \cancel{E}_T , and the estimated signal and background yields.

\sqrt{s} [TeV]	\cancel{E}_T [GeV]	\mathcal{L} [fb $^{-1}$]	N_{D5}	N_{bg}
7	350	4.9	73.3	1970 \pm 160
14	550	300	2500	2200 \pm 180
14	1100	3000	3200	1760 \pm 143
33	2750	3000	8.2 \cdot 10 4	1870 \pm 150
100	5500	3000	3.4 \cdot 10 6	2310 \pm 190

RESULTS FOR EFFECTIVE FIELD THEORIES

Given the expected background and uncertainties, we use the CLs method [21, 22] to calculate expected 90% confidence limits on contributions from new sources. Together with the estimated signal efficiencies, we calculate cross-section limits. As the predicted cross sections depend on M_* , we can therefore derive limits on M_* , see the top panel of Figs 3, 4, and 5. These are then translated in limits on the χ -nucleon cross section, see the right panel of Figs 3, 4, and 5.

In addition, we study the luminosity dependence of the results at $\sqrt{s} = 100$ TeV, see Figs 6, 7, and 8.

In Fig 9, we map to WIMP pair annihilation cross-section limits. Our predictions are compared to Fermi-LAT limits from a stacking analysis of Dwarf galaxies [29], including a factor of two to convert the Fermi-LAT limit from Majorana to Dirac fermions, and to projected sensitivities of CTA [28].

RESULTS FOR ON-SHELL MEDIATORS

The EFT approach is useful when the current facility does not have the necessary center-of-mass energy to produce on-shell mediators. The next-generation facility, however, may have such power.

In this section, we study the sensitivity of the proposed facilities to a model in which the heavy mediator is a Z' which couples to $\chi\bar{\chi}$ as well as $q\bar{q}$ [23–25]. We generate events as before, and measure the efficiency at parton level using simulated events.

The coupling of the Z' is a free parameter in this theory, but particularly interesting values are those which correspond to the limit of previous facilities on M_* . That is, an EFT model of the Z' interaction has

$$\frac{1}{M_*} = \frac{g_{Z'}}{M_{Z'}}$$

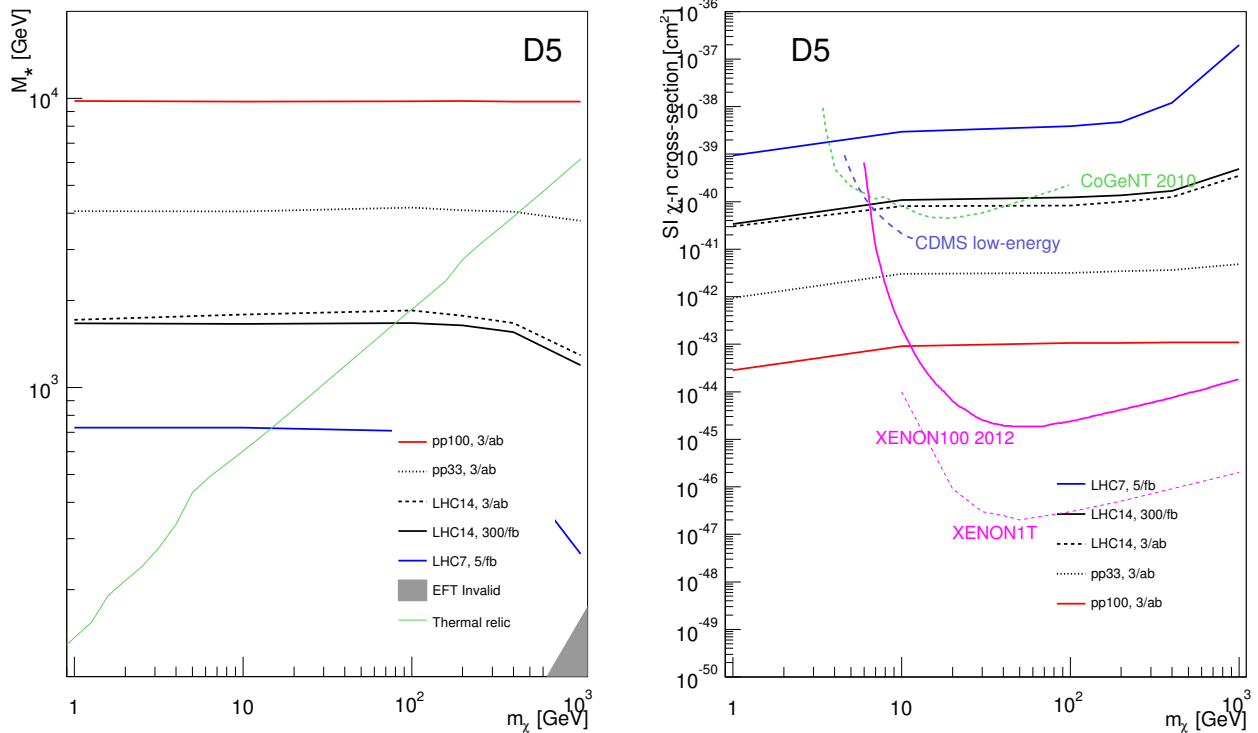


FIG. 3: Limits at 90% CL in M_* (left) and in the spin-independent WIMP-nucleon cross section (right) for different facilities using the D5 operator as a function of m_χ .

fixing the relationship between $g_{Z'}$ and $M_{Z'}$. Figure 10 shows the expected limits on the Z' model at a facility with $\sqrt{s} = 14$ TeV and $\mathcal{L} = 300 \text{ fb}^{-1}$, in terms of the cross section $\sigma(pp \rightarrow Z' \rightarrow \chi\bar{\chi}j)$ for $\cancel{E}_T > 550$ GeV and in terms of $g_{Z'}$. The g' expected limits can be compared to the curve with $g_{Z'} = \frac{M_{Z'}}{M_*}$; the cross-section limits can be compared to the predicted cross section assuming $g_{Z'} = \frac{M_{Z'}}{M_*}$.

Similar results for other facilities are shown in Figures 11, 12, and 13.

Acknowledgements

We acknowledge useful conversations with Roni Harnik and Patrick Fox. DW and NZ are supported by grants from the Department of Energy Office of Science and by the Alfred P. Sloan Foundation. The research of TMPT is supported in part by NSF grant PHY-0970171 and by the University of California, Irvine through a Chancellor's fellowship.

-
- [1] M. Beltran, D. Hooper, E. W. Kolb, Z. A. Krusberg, and T. M. Tait, *JHEP* **1009** (2010) 037, [arXiv:1002.4137 \[hep-ph\]](#).
 - [2] P. J. Fox, R. Harnik, J. Kopp, and Y. Tsai, *Phys.Rev.* **D85** (2012) 056011, [arXiv:1109.4398 \[hep-ph\]](#).
 - [3] J. Goodman, M. Ibe, A. Rajaraman, W. Shepherd, T. M. Tait, et al., *Phys.Rev.* **D82** (2010) 116010, [arXiv:1008.1783 \[hep-ph\]](#).
 - [4] G. Aad *et al.* [ATLAS Collaboration], *JHEP* **1304**, 075 (2013), [arXiv:1210.4491 \[hep-ex\]](#).
 - [5] S. Chatrchyan *et al.* [CMS Collaboration], *JHEP* **1209**, 094 (2012), [arXiv:1206.5663 \[hep-ex\]](#).
 - [6] G. Aad *et al.* [ATLAS Collaboration], *Phys. Rev. Lett.* **110**, 011802 (2013), [arXiv:1209.4625 \[hep-ex\]](#).
 - [7] S. Chatrchyan *et al.* [CMS Collaboration], *Phys. Rev. Lett.* **108**, 261803 (2012), [arXiv:1204.0821 \[hep-ex\]](#).
 - [8] Y. Bai and T. M. P. Tait, *Phys. Lett. B* **723**, 384 (2013), [arXiv:1208.4361 \[hep-ph\]](#).

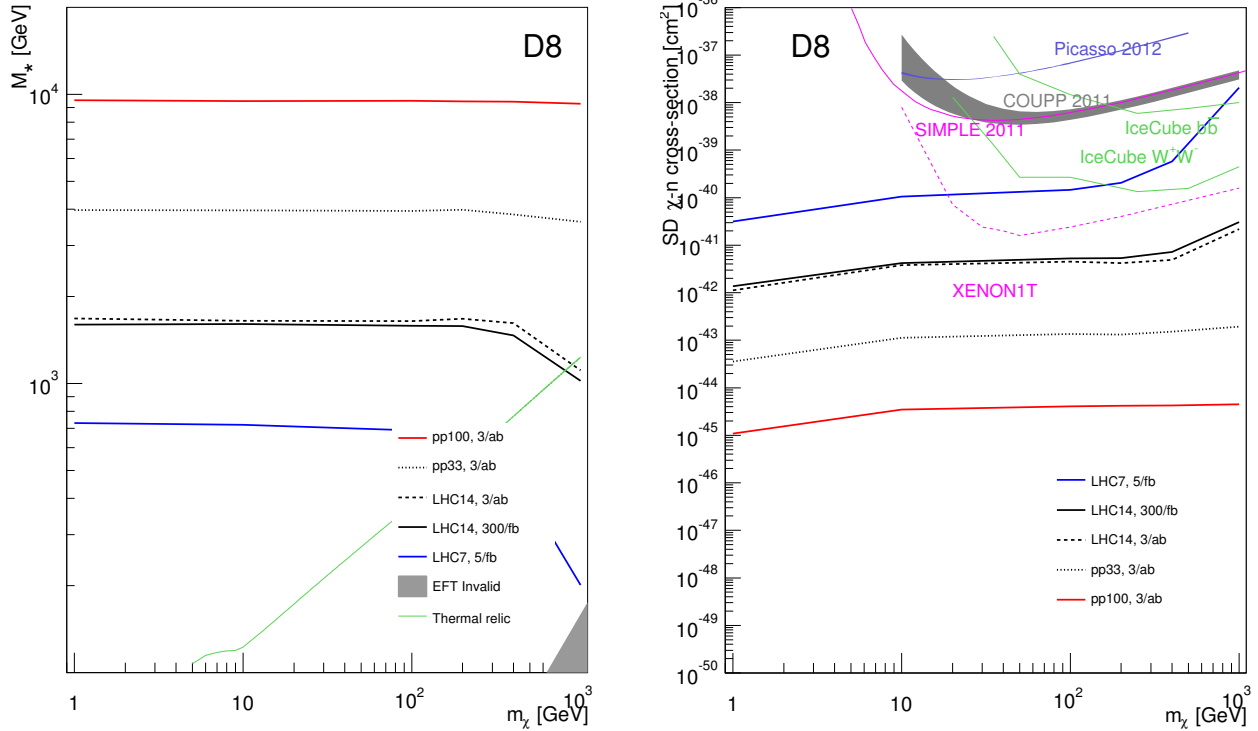


FIG. 4: Limits at 90% CL in M_* (left) and in the spin-dependent WIMP-nucleon cross section (right) for different facilities using the D8 operator as a function of m_χ .

- [9] G. Aad *et al.* [ATLAS Collaboration], *JHEP* **1203**, 128 (2013), [arXiv:1211.6096 \[hep-ex\]](#).
- [10] L. M. Carpenter, A. Nelson, C. Shimmin, T. M. P. Tait and D. Whiteson, *Phys. Rev. D* **87**, 074005 (2013), [arXiv:1212.3352 \[hep-ex\]](#).
- [11] M. Beltran, D. Hooper, E. W. Kolb and Z. C. Krusberg, *Phys. Rev. D* **80**, 043509 (2009), [arXiv:0808.3384 \[hep-ph\]](#).
- [12] W. Shepherd, T. M. P. Tait and G. Zaharijas, *Phys. Rev. D* **79**, 055022 (2009), [arXiv:0901.2125 \[hep-ph\]](#).
- [13] Q. -H. Cao, C. -R. Chen, C. S. Li and H. Zhang, *JHEP* **1108**, 018 (2011), [arXiv:0912.4511 \[hep-ph\]](#).
- [14] J. Goodman, M. Ibe, A. Rajaraman, W. Shepherd, T. M. P. Tait and H. -B. Yu, *Phys. Lett. B* **695**, 185 (2011), [arXiv:1005.1286 \[hep-ph\]](#).
- [15] Y. Bai, P. J. Fox and R. Harnik, *JHEP* **1012**, 048 (2010), [arXiv:1005.3797 \[hep-ph\]](#).
- [16] A. Rajaraman, W. Shepherd, T. M. P. Tait and A. M. Wijangco, *Phys. Rev. D* **84**, 095013 (2011), [arXiv:1108.1196 \[hep-ph\]](#).
- [17] R. C. Cotta, J. L. Hewett, M. P. Le and T. G. Rizzo, [arXiv:1210.0525 \[hep-ph\]](#).
- [18] F. J. Petriello, S. Quackenbush and K. M. Zurek, *Phys. Rev. D* **77**, 115020 (2008), [arXiv:0803.4005 \[hep-ph\]](#).
- [19] Y. Gershtein, F. Petriello, S. Quackenbush and K. M. Zurek, *Phys. Rev. D* **78**, 095002 (2008), [arXiv:0809.2849 \[hep-ph\]](#).
- [20] N. Zhou, D. Berge and D. Whiteson, *Phys. Rev. D* **87**, 095013 (2013), [arXiv:1302.3619 \[hep-ex\]](#).
- [21] A. L. Read, *J.Phys.G* **G28** (2002) 2693–2704.
- [22] T. Junk, *Nucl. Instrum. Methods A* **434**, 425 (1999), [arXiv:9902006 \[hep-ex\]](#).
- [23] H. An, X. Ji and L. -T. Wang, *JHEP* **1207**, 182 (2012), [arXiv:1202.2894 \[hep-ph\]](#).
- [24] M. T. Frandsen, F. Kahlhoefer, A. Preston, S. Sarkar and K. Schmidt-Hoberg, *JHEP* **1207**, 123 (2012) [[arXiv:1204.3839 \[hep-ph\]](#)].
- [25] I. M. Shoemaker and L. Vecchi, *Phys. Rev. D* **86**, 015023 (2012) [[arXiv:1112.5457 \[hep-ph\]](#)].
- [26] J. Alwall, M. Herquet, F. Maltoni, O. Mattelaer, and T. Stelzer, *JHEP* **1106** (2011) 128, [arXiv:1106.0522 \[hep-ph\]](#).
- [27] T. Sjostrand, S. Mrenna, and P. Z. Skands, *JHEP* **0605** (2006) 026, [arXiv:hep-ph/0603175 \[hep-ph\]](#).
- [28] M. Doro *et al.*, *Astropart.Phys.* **43** (2013) 189, [arXiv:1208.5356 \[astro-ph\]](#).
- [29] Fermi-LAT Collaboration, M. Ackermann *et al.*, *Phys.Rev.Lett.* **107** (2011) 241302, [arXiv:1108.3546 \[astro-ph.HE\]](#).

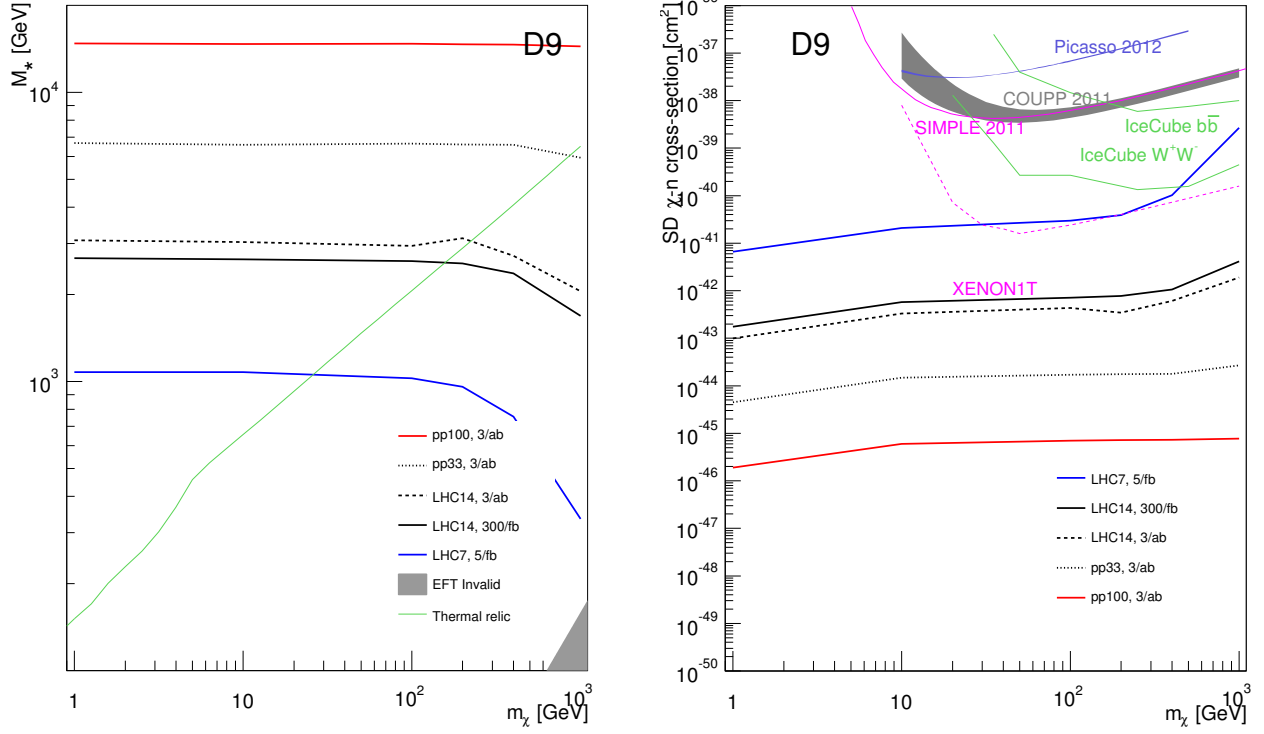


FIG. 5: Limits at 90% CL in M_* (left) and in the spin-dependent WIMP-nucleon cross section (right) for different facilities using the D9 operator as a function of m_χ .

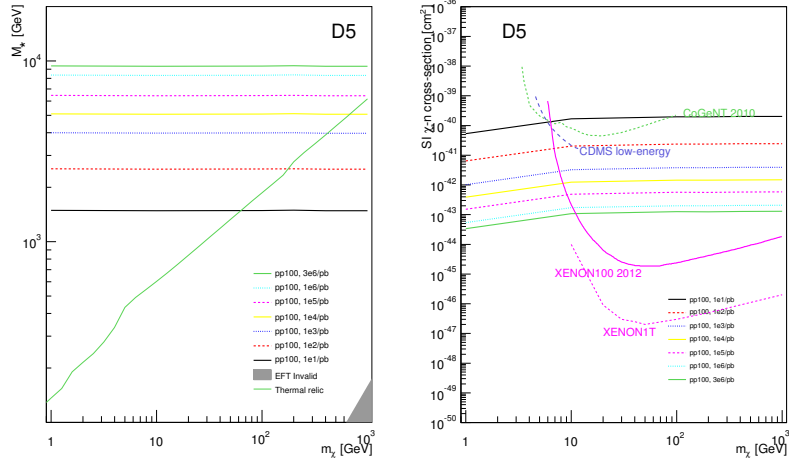


FIG. 6: Limits at 90% CL in M_* (left) and in the spin-independent WIMP-nucleon cross section (right) for increasing luminosity using the D5 operator as a function of m_χ .

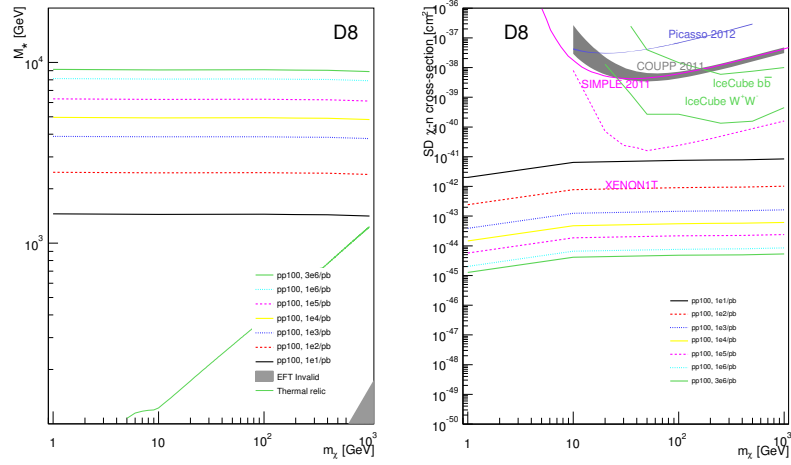


FIG. 7: Limits at 90% CL in M_* (left) and in the spin-dependent WIMP-nucleon cross section (right) for increasing luminosity using the D8 operator as a function of m_χ .

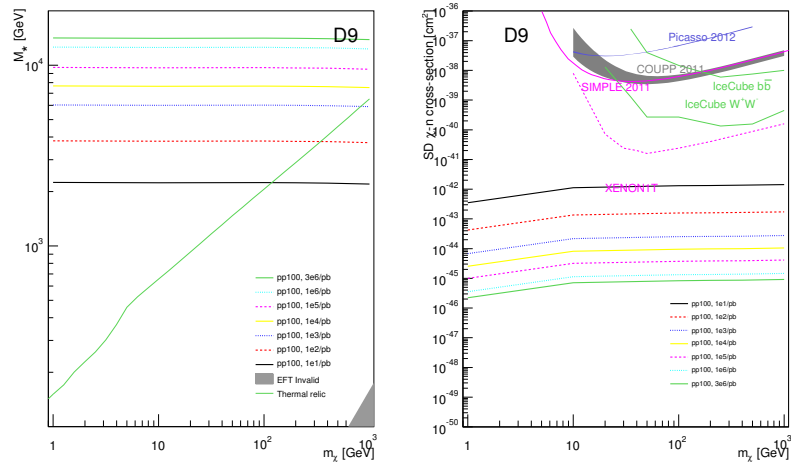


FIG. 8: Limits at 90% CL in M_* (left) and in the spin-dependent WIMP-nucleon cross section (right) for increasing luminosity using the D9 operator as a function of m_χ .

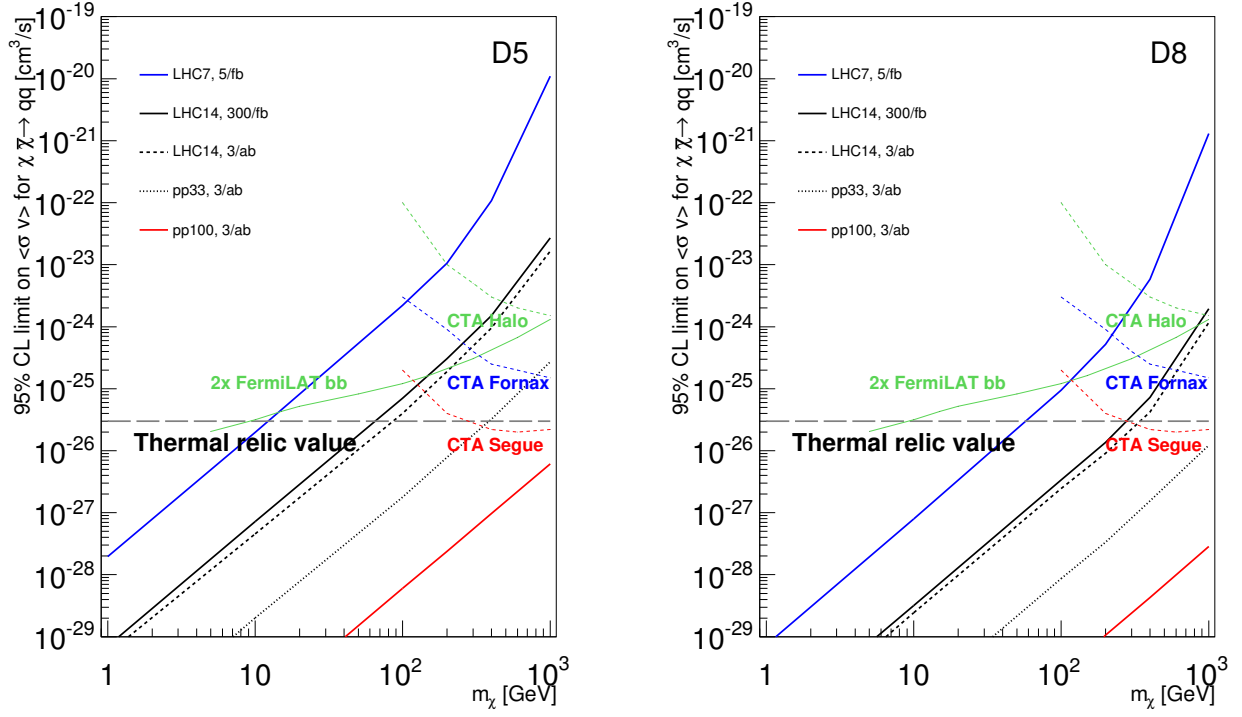


FIG. 9: Limits at 95% CL on WIMP pair annihilation for different facilities using the D5 (left) or D8 (right) operator as a function of m_χ .

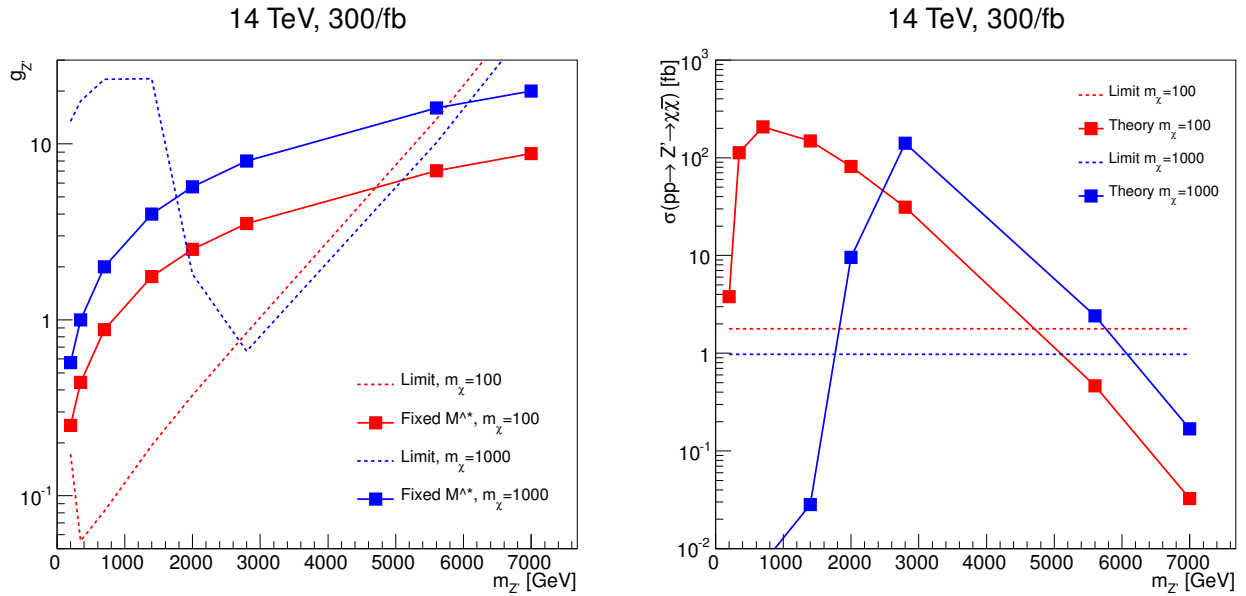


FIG. 10: Sensitivity at $\sqrt{s} = 14$ TeV, $\mathcal{L} = 300$ fb $^{-1}$ to a dark matter pairs produced through a real Z' mediator. Left, expected limits on the coupling $g_{Z'}$ versus Z' mass for two choices of m_χ for events with $\cancel{E}_T > 550$ GeV; also shown are the values of $g_{Z'}$ which satisfy $g'/m_{Z'} = 1/M_*$, where M_* are limits from $\sqrt{s} = 7$ TeV, $\mathcal{L} = 5$ fb $^{-1}$. Right, production cross section as a function of Z' mass, compared to expected limits, where $g_{Z'}$ depends on $m_{Z'}$ as in the left pane.

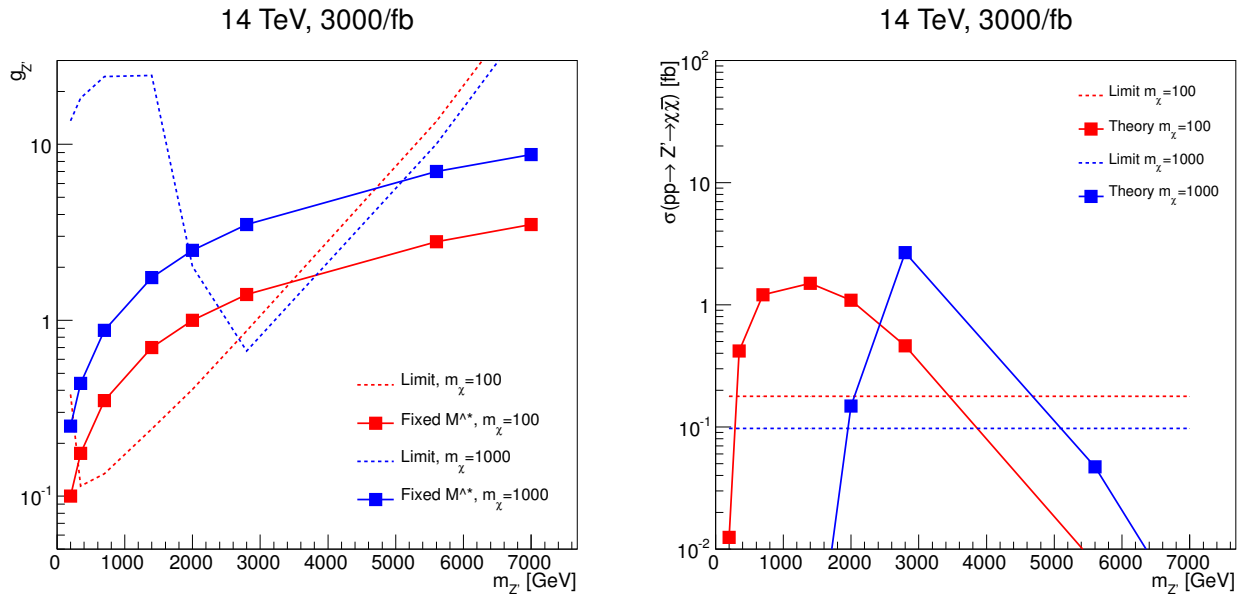


FIG. 11: Sensitivity at $\sqrt{s} = 14$ TeV, $\mathcal{L} = 3000$ fb $^{-1}$ to a dark matter pairs produced through a real Z' mediator. Left, expected limits on the coupling $g_{Z'}$ versus Z' mass for two choices of m_χ for events with $\cancel{E}_T > 1100$ GeV; also shown are the values of $g_{Z'}$ which satisfy $g'/m_{Z'} = 1/M_*$, where M_* are limits from $\sqrt{s} = 14$ TeV, $\mathcal{L} = 300$ fb $^{-1}$. Right, production cross section as a function of Z' mass, compared to expected limits, where $g_{Z'}$ depends on $m_{Z'}$ as in the left pane.

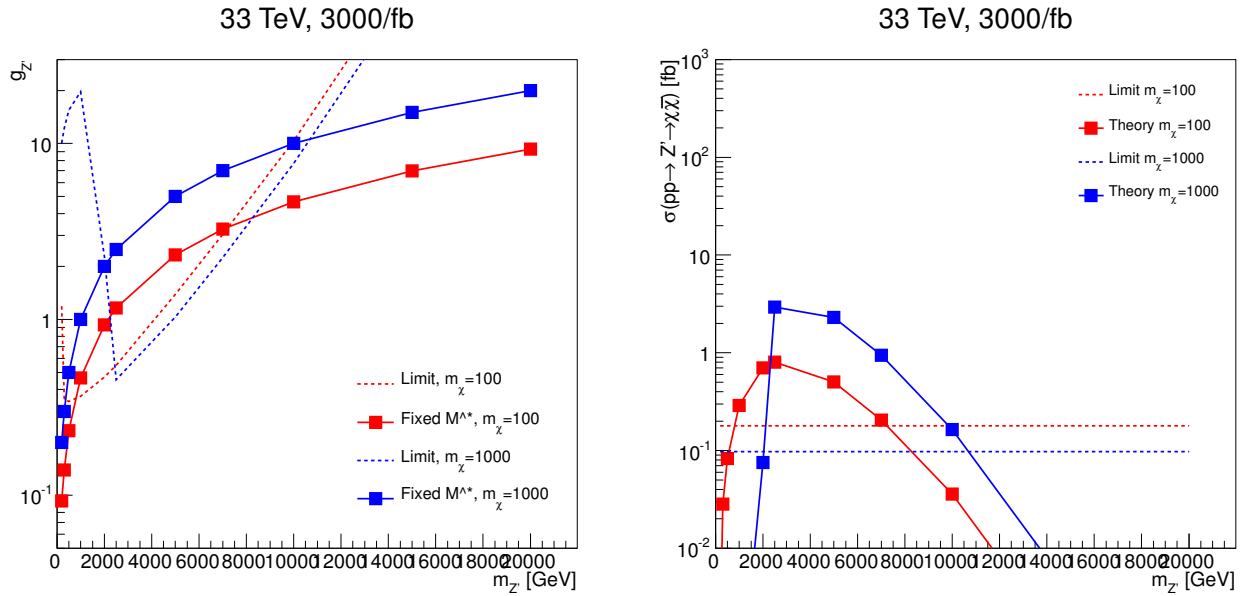


FIG. 12: Sensitivity at $\sqrt{s} = 33$ TeV, $\mathcal{L} = 3000$ fb $^{-1}$ to a dark matter pairs produced through a real Z' mediator. Left, expected limits on the coupling $g_{Z'}$ versus Z' mass for two choices of m_χ for events with $\cancel{E}_T > 2750$ GeV; also shown are the values of $g_{Z'}$ which satisfy $g'/m_{Z'} = 1/M_*$, where M_* are limits from $\sqrt{s} = 14$ TeV, $\mathcal{L} = 3000$ fb $^{-1}$. Right, production cross section as a function of Z' mass, compared to expected limits, where $g_{Z'}$ depends on $m_{Z'}$ as in the left pane.

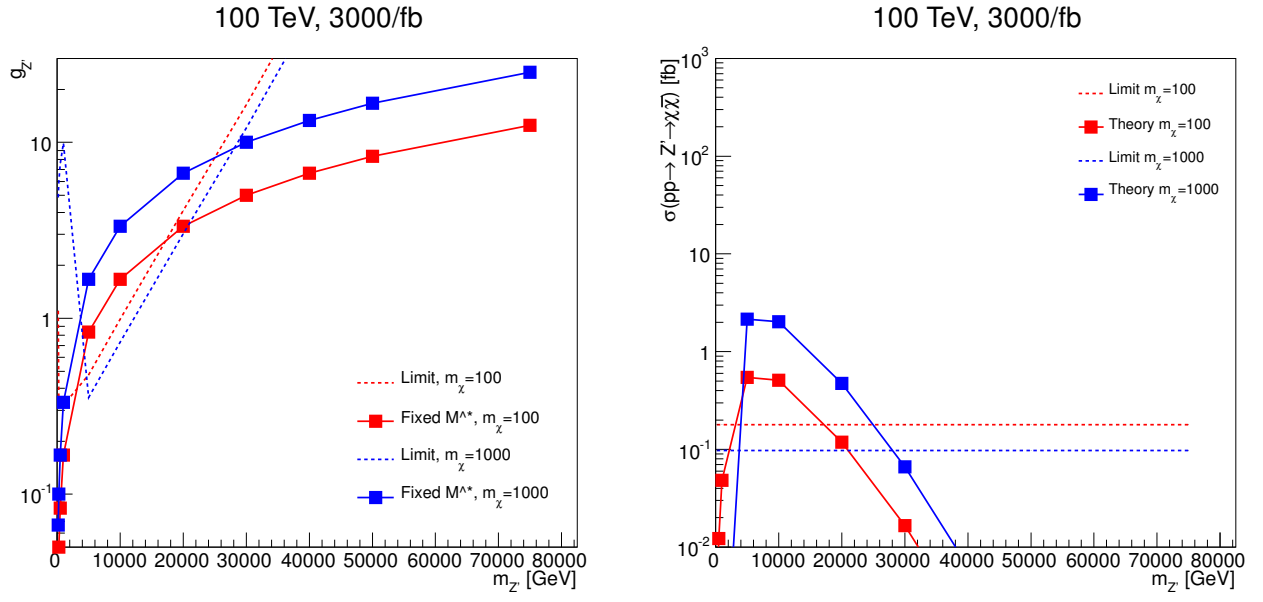


FIG. 13: Sensitivity at $\sqrt{s} = 100$ TeV, $\mathcal{L} = 3000$ fb $^{-1}$ to a dark matter pairs produced through a real Z' mediator. Top, expected limits on the coupling $g_{Z'}$ versus Z' mass for two choices of m_{χ} for events with $\cancel{E}_T > 5500$ GeV; also shown are the values of $g_{Z'}$ which satisfy $g'/m_{Z'} = 1/M_*$, where M_* are limits from $\sqrt{s} = 33$ TeV, $\mathcal{L} = 3000$ fb $^{-1}$. Bottom, production cross section as a function of Z' mass, compared to expected limits, where $g_{Z'}$ depends on $m_{Z'}$ as in the top pane.